

# Constraining Stellar-mass Black Hole Mergers in AGN Disks Detectable with LIGO

Barry McKernan 1,2,3 , K. E. Saavik Ford 1,2,3 , J. Bellovary 2,4 , N. W. C. Leigh 2, Z. Haiman 5, B. Kocsis 6, W. Lyra 2,5 , M.-M. Mac Low 2, B. Metzger 5, M. O'Dowd 2,3,7 , S. Endlich 8, and D. J. Rosen 1, Department of Science, CUNY-BMCC, 199 Chambers St., New York, NY 10007, USA 2, Department of Astrophysics, American Museum of Natural History, Central Park West, New York, NY 10028, USA 3, CUNY Graduate Center, 365, 5th Avenue, New York, NY 10016, USA 4, Department of Physics, CUNY-QCC, Bayside, New York, NY 1034, USA 5, Columbia Astrophysics Laboratory, Columbia University, New York, NY 10027, USA 6, Institute of Physics, Eötvös University, Budapest 1117, Hungary 7, Department of Physics, CUNY-Lehman, New York, NY 10468, USA 8, Stanford Institute for Theoretical Physics, Stanford University, CA 94306, USA Received 2018 January 29; revised 2018 July 11; accepted 2018 August 14; published 2018 October 15

### **Abstract**

Black hole (BH) mergers detectable with the Laser Interferometer Gravitational-wave Observatory (LIGO) can occur in active galactic nucleus (AGN) disks. Here we parameterize the merger rates, the mass spectrum, and the spin spectrum of BHs in AGN disks. The predicted merger rate spans  $\sim 10^{-3}-10^4\,\mathrm{Gpc}^{-1}\,\mathrm{yr}^{-1}$ , so upper limits from LIGO ( $<212\,\mathrm{Gpc}^{-1}\,\mathrm{yr}^{-1}$ ) already constrain it. The predicted mass spectrum has the form of a broken power law, consisting of a pre-existing BH power-law mass spectrum and a harder power-law mass spectrum resulting from mergers. The predicted spin spectrum is multipeaked with the evolution of retrograde spin BHs in the gas disk playing a key role. We outline the large uncertainties in each of these LIGO observables for this channel and we discuss ways in which they can be constrained in the future.

Key words: accretion, accretion disks – binaries: close – black hole physics – galaxies: active – gravitational waves

#### 1. Introduction

The gravitational-wave (GW) events detected by the Advanced Laser Interferometer Gravitational-wave Observatory (LIGO) correspond to the merger of stellar-mass black holes (BHs) and are considerably more massive than those observed in our own Galaxy (Abbott et al. 2016a). The upper end of the range of BH merger rates derived from LIGO observations of  $212 \,\mathrm{Gpc}^{-3} \,\mathrm{yr}^{-1}$  (Abbott et al. 2016b) requires the consideration of locations where BH mergers can occur faster than expected from GW emission alone. Among the first few LIGO detections are possible low value spin or misaligned spins, which may be problematic for models of binary evolution (O'Shaughnessey et al. 2017). While BHs with larger than expected masses can occur naturally in the field (Belczynski et al. 2010; deMink & Mandel 2016) and in globular clusters (Breen & Heggie 2013; Rodriguez et al. 2016a, 2018; Wang et al. 2016), they are more likely to form in regions with concentrations of BHs, such as galactic nuclear star clusters (Hopman & Alexander 2006; O'Leary et al. 2009; Antonini & Rasio 2016; Rodriguez et al. 2016b). Massive gas disks in active galactic nuclei (AGNs) provide natural locations for gas accretion and repeated mergers because the gas disk can drive migration of BHs toward migration traps, reduce the inclination of intersecting orbits, enable binary formation, and harden existing binaries. Together, these effects can result in the rapid increase in the mass of embedded BHs, potentially to observed values (e.g., McKernan et al. 2012, 2014; Bellovary et al. 2016; Bartos et al. 2017; Stone et al. 2017).

In this paper, we parameterize the expected merger rate, and the mass and spin distributions from this channel for comparison with the LIGO observations, and we discuss how observations and simulations can constrain these predictions.

#### 2. Model Outline

Galactic nuclei likely contain some of the densest concentrations of BHs in the universe (e.g., Morris 1993; Miralda-Escudé & Gould 2000; Hailey et al. 2018, and references therein), so it is natural to look for BH mergers in galactic nuclei (O'Leary et al. 2009; McKernan et al. 2012; Antonini 2014). While BH binary mergers can occur at modestly enhanced rates (compared to the field) in nuclear star clusters just from dynamical binary hardening (Antonini & Rasio 2016; Rodriguez et al. 2016b), or capture from single–single (O'Leary et al. 2009) and binary–single encounters (Samsing et al. 2014), a dense nuclear disk of gas can greatly accelerate the rate of BHB formation and merger (McKernan et al. 2012, 2014).

The simplest picture of this LIGO channel begins with a spherical distribution of BHs, stars, and other stellar remnants orbiting in the central pc<sup>3</sup> of a galactic nuclei around a supermassive black hole (SMBH). Next, around the SMBH, we add a massive gas disk, which can be geometrically thin or thick. A fraction  $f_{co}$  of the initial number of BHs in the nucleus  $N_{\rm BH}$ , will have orbits coincident with the disk and approximately half of these orbits should be retrograde compared to the disk gas. Yet another fraction  $f_{\rm g}$  of the population  $N_{\rm BH}$ intersects the disk on their orbits and are ground down into the plane of the disk within the AGN disk lifetime ( $\tau_{AGN}$ ). Thus an overall fraction  $f_d = f_{co} + f_{g}$  of nuclear BHs end up embedded in the disk, and quickly have their orbits damped and circularized by gas drag (e.g., McKernan et al. 2012). The net torques from disk gas causes BHs to migrate within the disk and encounter each other at low relative velocities (McKernan et al. 2012; Bellovary et al. 2016). BH binaries that form in the disk are expected to merge efficiently due to gas torques (e.g., Haiman et al. 2009; Stahler 2010; Baruteau et al. 2011; Kocsis et al. 2011; McKernan et al. 2011, 2012). BH mergers may

Table 1
Parameter Ranges in Equation (1)

Parameter	Lower	Upper
$N_{\rm GN}^{\rm a}({\rm Mpc}^{-3})$	$4 \times 10^{-3}$	$10^{-2}$
$N_{\rm BH}^{\rm b}({\rm pc}^{-3})$	$10^{4}$	$10^{6}$
$f_{\rm AGN}^{^{^{}}}$	0.01	0.3
$f_b$	0.01	0.2
$f_b f_d^{\mathbf{d}}$	0.01	0.7
$\tau_{AGN}(Myr)$	1	100
$\epsilon$	0.5	2
$\mathcal{R}(\mathrm{Gpc}^{-3}\mathrm{yr}^{-1})$	$10^{-3}$	$10^{4}$

**Notes.** Range of parameters in Equation (1) and range of merger rate (see the text).

preferentially occur in convergence zones containing migration traps (Bellovary et al. 2016), which occur in semirealistic models of AGN disks (Sirko & Goodman 2003; Thompson et al. 2005). Multiple objects trapped in such orbits collide efficiently rather than being ejected (Horn et al. 2012; A. Secunda et al. 2018, in preparation). In this paper, we examine what constraints can be put on the merger rate and the BH spin and mass distributions for this AGN channel.

# 3. Rate of BH Binary Mergers in AGN Disks

We parameterize the rate of BH–BH mergers in AGN disks simply as:

$$\mathcal{R} = \frac{N_{\rm GN} N_{\rm BH} f_{\rm AGN} f_d f_b \epsilon}{\tau_{\rm AGN}},\tag{1}$$

where  $N_{\rm GN}$  (Mpc<sup>-3</sup>) is the average number density of galactic nuclei in the universe,  $f_{\rm AGN}$  is the fraction of galactic nuclei that have active AGNs that last for time  $\tau_{\rm AGN}$ ,  $f_d = f_{\rm co} + f_g$  is the fraction of nuclear BHs that end up in the disk,  $f_b$  is the fraction of BHs in BH–BH binaries in the disk, and  $\epsilon$  represents the fractional change in number  $N_{\rm BH}$  of BHs in the central region ( $\sim$ pc<sup>3</sup>) over a full AGN duty cycle<sup>9</sup>  $\mathcal R$  can be parameterized as:

$$\mathcal{R} = 12 \text{ Gpc}^{-3} \text{ yr}^{-1} \frac{N_{\text{GN}}}{0.006 \text{ Mpc}^{-3}} \frac{N_{\text{BH}}}{2 \times 10^4} \frac{f_{\text{AGN}}}{0.1} \times \frac{f_d}{0.1} \frac{f_b}{0.1} \frac{\epsilon}{10 \text{ Myr}} \left( \frac{\tau_{\text{AGN}}}{10 \text{ Myr}} \right)^{-1}.$$
 (2)

However, if we want to constrain the contributions of this channel to LIGO observations, it is much more useful to show the allowed range of  $\mathcal R$  and the range of each of the contributing factors from Equation (1), which we list in Table 1.

The  $N_{\rm GN}$  lower limit corresponds to galaxies with stellar mass greater than or equal to that of the Milky Way (Baldry et al. 2012) as measured from the Schechter function fits to galaxy luminosity functions (e.g., Cole et al. 2001). The  $N_{\rm GN}$ upper limit corresponds to dwarf galaxies with stellar mass  $>10^9 M_{\odot}$  (Baldry et al. 2012), which includes all locally observed SMBH ( $\geqslant 10^5 M_{\odot}$ ) inferred from  $M - \sigma$  studies of galaxies and dwarf galaxies (Reines & Volonteri 2015). Note that if  $N_{GN}$  were in fact lower as in, e.g., Georgakakis et al. (2015) and Volonteri et al. (2016), then the lower bound to  $N_{\rm GN}$ as estimated by us could drop by several orders of magnitude, which would obviously impact the rate of range. However, we prefer optical selection of galaxies to derive  $N_{\rm GN}$  rather than X-ray selection of AGNs, which would fold in  $f_{AGN}$  implicitly (but only for X-ray bright AGNs) and incur a series of observational biases (including Compton-thick absorption, bias against LINERs etc.) which would undercount the actual AGN number.

Chandra observations of quiescent X-ray binaries around SgrA\* (Hailey et al. 2018) give the strongest observational constraint on  $N_{\rm BH}$  in Table 1. Generozov et al. (2018) extrapolate a population of  $N_{\rm BH} \gtrsim 10^4$  BHs within the central parsec of the Galaxy. This estimate is consistent with predictions from a range of mechanisms, including  $\sim 10^4$  from in situ formation (Generozov et al. 2018),  $\gtrsim 10^4$  from globular cluster infall (Antonini 2014), and  $\sim 2.5 \times 10^4$  from direct BH infall (Miralda-Escudé & Gould 2000). If SgrA\* is typical for low-powered AGNs (which dominate  $f_{\rm AGN}$ ), then  $N_{\rm BH} \sim 10^4$  is an appropriate lower limit.  $N_{\rm BH} \sim 10^{5}$  is probably a reasonable upper limit for a Galactic center like ours, assuming multiple mechanisms contribute significantly to nuclear BH population. We will take a strict upper limit of  $N_{\rm BH} \sim 10^6$  from simulations (Antonini 2014) for populations around much more massive SMBHs with recent starbursts and/or cluster decay.

The lower limit to  $f_{\rm AGN}$  assumes only quasar disks are efficient BH merger sites and  $f_{\rm AGN} \sim 0.3$  assumes all LINER galactic nuclei (Ho 2008) consist of advection dominated accretion flows (ADAFs) with high accretion rate (Paczynski & Witta 1980; Narayan & Yi 1995; Lasota et al. 2016), capable of driving BH mergers.

The binary fraction of BHs  $f_b$  has been estimated to be as high as  $f_b \sim 0.2$  (Antonini 2014), but dynamically hot environments such as star clusters, could actually yield very low binary fractions  $f_b \leq 0.01$  over time in the absence of gas (Miller & Davies 2012; Leigh et al. 2016) due to the large number of "ionizing" interactions, so we choose  $f_b = [0.01, 0.2]$  in Table 1. More recent work by us (Secunda et al. 2018) implies that the binary fraction in the inner disk can average  $f_b \sim 0.6$ –0.8 in 1 Myr, so  $f_b$  on average could even be as high as  $f_b \sim 0.3$  across the whole disk. However, since the AGN disk could persist for >1 Myr  $f_b \sim 0.2$  represents a reasonable upper limit.

Reasonable estimates of  $\tau_{\rm AGN}$  span 0.1–100 Myr (Haehnelt & Rees 1993; King & Nixon 2015; Schawinski et al. 2015).  $\mathcal R}$  will be highest if AGN episodes are short lived but frequently repeated and efficient at BH mergers. These circumstances ensure that there are multiple opportunities for BHs in a galactic nucleus to encounter each other at low relative velocity and merge in a disk.

From Table 1, the allowed range from Equation (1) is  $\mathcal{R}\sim 10^{-3}\text{--}10^4~\text{Gpc}^{-3}~\text{yr}^{-1}$ . The upper bound to the LIGO BH binary merger rate of  $\sim\!240~\text{Gpc}^{-3}~\text{yr}^{-1}$  already rules out upper

<sup>&</sup>lt;sup>a</sup> From Baldry et al. (2012).

<sup>&</sup>lt;sup>b</sup> From Miralda-Escudé & Gould (2000), Antonini (2014), Hailey et al. (2018). <sup>c</sup>  $f_{\rm AGN} \sim 0.1$  for Seyfert AGNs (Ho 2008).  $f_{\rm AGN} \sim 0.3$  with all LINERs and other low luminosity AGNs.

<sup>&</sup>lt;sup>d</sup>  $f_d = f_{\rm co} + f_g$ .  $f_{\rm co}$  comes from h/R, the disk aspect ratio.  $h/R \sim 0.01$ –0.1 (Sirko & Goodman 2003).  $h/R \sim 10^{-3}$ –0.1 (Thompson et al. 2005).  $h/R \sim 0.1$ –0.7 in super-Eddington ADAFs (Lasota et al. 2016).  $f_g$  depends on h/R,  $\rho_{\rm disk}$  and  $\tau_{\rm AGN}$ .

If  $\epsilon \sim 1$ , then  $N_{\rm BH}$  is approximately conserved between AGN episodes. If  $\epsilon(>) < 1 \ N_{\rm BH}$  (grows) shrinks between AGN phases due to the net effect of mergers, infall of new BHs, stellar evolution, etc.

limits to most parameters in Table 110 and allows actual astrophysical limits to be placed on models of AGN disks by LIGO BH merger detections. Future observational constraints and simulation results will, however, be required to figure out which upper limits are ruled out by LIGO. For example, the upper limit to  $N_{\rm GN}$  could be reduced by contrasting activity rates as a function of galactic mass in a complete sample. The inferred  $N_{\rm BH}$  can be constrained via population studies of the X-ray emission from binaries around Sgr A\* and in M31, as well as via dynamics studies of the number density of BHs allowed from the orbital parameters of stars in galactic nuclei. The upper limit on  $f_{AGN}$  can be reduced if we can observationally distinguish between high- and low-accretion rate LINERs. Simulations that include a spherical component of individual stars and BHs as well as migrating objects in the disk are required to properly constrain  $f_b$ . Encounters between objects from the spherical dynamical component and the disk dynamical component will occur at relatively high velocity and can therefore ionize sufficiently soft, large radius, binaries. Thus, in order for  $f_b$  to be moderately large in this channel, we require  $f_{\varrho}$  to be large, since otherwise the rate of ionizing encounters can ionize binaries (Leigh et al. 2017). So limits on  $f_g$  from semianalytic approaches or simulations (Kennedy et al. 2016) can also help constrain  $f_b$ .

Uncertainties in  $\mathcal{R}$  are dominated mainly by a lack of knowledge of the distribution and number of BHs in galactic nuclei, how efficiently gas disks can grind-down orbits, and whether geometrically thick disks can efficiently merge BHs. Understanding multiple-object migration and the role of retrograde orbiters is another key area for future work.

### 4. Constraining BH Masses

By merging BHs in AGN disks, we expect "overweight" BHs to result (McKernan et al. 2012). To investigate the range of BH masses involved in mergers in this channel, we use a toy model calculation of the evolution of a population of BHs embedded and migrating in an AGN disk. We made many simplifying assumptions: there are no BH binaries to begin with  $(f_b=0)$ , BHs remain in the disk after merger, tertiary encounters are neglected, no BHs merge with the SMBH, no new BHs are added to the population  $(f_g=0)$  and we ignore mass growth due to gas accretion. We began with a uniform distribution of BHs drawn from a Kroupa (2002) initial mass function  $N_{\rm BH}(M) \propto M^{-\gamma_0}$ , with  $\gamma_0=2.3$  distributed over three mass bins  $(5, 10, 15\,M_\odot)$  and chose normalization  $N_{\rm BH}(5\,M_\odot)=10^3$ .

A BH on a prograde orbit in an AGN disk with mass  $M_1$  will migrate on a (Type I) timescale (Paardekooper et al. 2010; McKernan et al. 2012)

$$t_{\text{mig}} \approx 38 \text{ Myr} \left(\frac{N}{3}\right)^{-1} \left(\frac{R_{\text{b}}}{10^{4} r_{\text{g}}}\right)^{-1/2} \left(\frac{M_{1}}{5 M_{\odot}}\right)^{-1} \times \left(\frac{h/R_{b}}{0.02}\right)^{2} \left(\frac{\Sigma}{10^{5} \text{ kg m}^{-2}}\right)^{-1} \left(\frac{M_{\text{SMBH}}}{10^{8} M_{\odot}}\right)^{3/2}, \tag{3}$$

where N is a numerical factor of the order of 3. So the toy model population outlined above will evolve over time. If  $10^3$ 

BHs are uniformly distributed across a disk of radius  $R_d \sim 10^5 r_g$ ,  $(r_g = GM_{\rm SMBH}/c^2)$ , BH orbits are separated by  $\sim 10^2 r_g$  on average. This separation could be closed in  $\sim 0.4$  Myr from Equation (3). Our initial distribution of singleton BHs separated by  $\sim 10^2 r_g$  on average will therefore evolve from  $f_b = 0$  toward  $f_b \sim 0.5$  within  $\sim 0.4$  Myr due to migration. The probability of encounter between BHs of masses  $M_1$ ,  $M_2$  in time  $\Delta t$  is

$$P(M_1|M_2) \propto \frac{N(M_1)N(M_2)}{t_{\text{mig}}(M_1)t_{\text{mig}}(M_2)}.$$
 (4)

When a pair of BHs approaches within their binary Hill radius  $R_H = (q/3)^{1/3} R_b$ , where q is the binary mass ratio and  $R_b$  is the radius of the binary center of mass, gas drag can cause them to merge rapidly. Baruteau et al. (2011) showed that binary semimajor axis  $a_b$  halves due to gas drag in only 200 (1000) orbits about the binary center of mass for a retrograde (prograde) binary compared to gas velocity. Using this result, a BH binary with  $a_b = R_H$  at  $R_b \sim 10^3 r_g$  has a characteristic timescale for binary hardening of 0.4 kyr (8 kyr) in the retrograde(prograde) case. Only 20–25 such halvings (corresponding to  $\sim 0.1-0.2 \,\mathrm{Myr}$ , naively assuming a constant gas hardening rate) would shrink  $a_b$  sufficiently that GW emission takes over and the merger happens promptly. The gas hardening rate may be even faster than this estimate since more gas enters the binary's Hill sphere as it shrinks (Baruteau et al. 2011), which may pump binary eccentricity. However, gas torques may decrease in efficiency once the binary has hardened sufficiently that the binary velocity is substantially supersonic compared to most gas within the Hill radius (Sánchez-Salcedo & Chametla 2014). For our toy model, we therefore assume  $\sim 0.1 \,\mathrm{Myr}$  is the minimum gas hardening timescale to merger, but we note that the actual gas hardening timescale could take up to an order of magnitude longer.

In our toy model, if the typical time for a BH to encounter another BH in the disk is  $\sim$ 0.4 Myr, then adding an additional  $\sim$ 0.1–1 Myr for a gas hardening timescale yields a characteristic time to merger of  $\sim$ 0.5–1.5 Myr in our model. So, we expect that around half the initial population of our toy model will have encountered each other and merged in this time. In calculating the evolution of our toy model, we chose  $\Delta t \sim 0.1$ –0.3 Myr to correspond to a time when  $\sim$ 10% of the initial population of lowest mass BHs (5  $M_{\odot}$ ) have encountered each other and merged. All other encounters are normalized to this encounter rate. For simplicity, we assume all binaries that formed in  $\Delta t$  merge within that time, and we neglect the mass-energy loss from the mergers. After  $\Delta t$ , all BHs that merged are removed from their original mass bins, and the newly merged object is added to the appropriate mass bin.

Figure 1 demonstrates the simplistic evolution expected as the initial BH distribution (black line) evolves to the red curve in time step  $\Delta t \sim 0.1\text{--}0.3$  Myr, where  $\sim\!10\%$  of the lowest mass BHs in the initial (black) distribution have merged. The red curve evolves to the blue curve after an additional  $\Delta t' \sim 0.2\text{--}0.6$  Myr, when  $\sim\!10\%$  of the lowest mass BH on the red curve are expected to merge. The BH mass distribution in our toy model flattens from  $\gamma_0=2.3$  to  $\gamma\sim2$  as low-mass BHs are consumed.

Now assume that BHs from the nondisk spherical population, interact with the disk and their orbits are ground down into the disk, i.e.,  $f_g > 0$ . The addition of some of the (initially)

 $<sup>^{10}</sup>$  The LIGO rate upper bound places a lower limit on  $\epsilon$ , since a small value of  $\epsilon$  suggests most BHs in AGNs are consumed in mergers and would imply a much greater  $\mathcal R$  than observed.

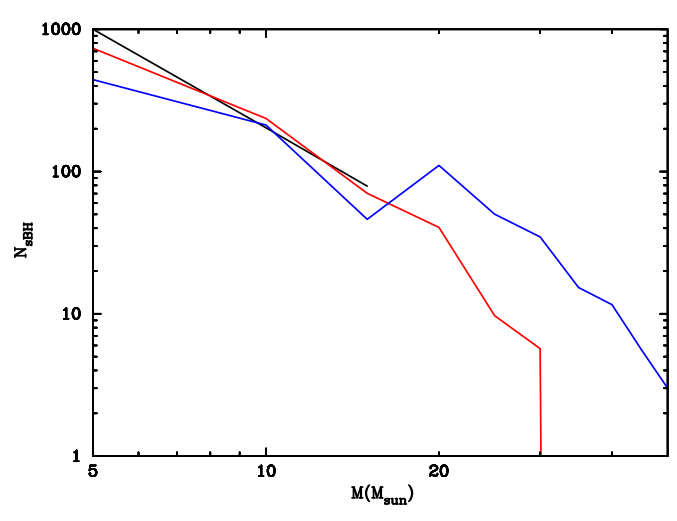


**Figure 1.** Evolution of an initial  $5{\text -}15\,M_\odot$  BH mass distribution (black curve) in an AGN disk based on a toy merger model. Black curve corresponds to the initial BH mass distribution. Red and blue curves show the evolution of the distribution after timesteps corresponding to  $\Delta t \approx 0.1{\text -}0.3\,\text{Myr}$  and  $\Delta t' \sim 0.2{\text -}0.6\,\text{Myr}$  respectively (see the text). A choice of heavier initial mass range will alter upper mass limits.

spherical BH population to the disk will support the BH mass distribution in the disk at the low-mass end. So an initial power-law distribution  $\propto M^{-\gamma_0}$  of BH mass will evolve toward a broken-power-law distribution of the form

$$N_{\rm BH} \propto \begin{cases} N_1 M^{-\gamma_1} \text{ for } M < M_{\rm break} \\ N_2 M^{-\gamma_2} \text{ for } M > M_{\rm break} \end{cases}$$
 (5)

where  $\gamma_2 < \gamma_1$ ,  $N_1/N_2 \sim (f_g/f_{co})$ , where  $f_{co}$  is the fraction of BHs initially in the disk and on average  $f_g$  is the fraction of BHs ground down into the disk over  $\tau_{AGN}/2$  and  $M_{break}$  lies near the upper end of the initial mass range ( $\sim 15~M_{\odot}$  in our toy model).

In order to include gas accretion in this toy model, we assumed a gas accretion rate for BHs on (retrograde, prograde) orbits of  $\dot{M}_1 \sim [10^{-2}, 1] \dot{M}_{\rm Edd}$ , where

$$\dot{M}_{\rm Edd} = \frac{4\pi G M_1 m_p}{\eta c}$$

$$\approx 2.2 \times 10^{-7} \frac{M_{\odot}}{\rm years} \left(\frac{\eta}{0.1}\right)^{-1} \left(\frac{M_1}{10 M_{\odot}}\right) \tag{6}$$

is the Eddington mass accretion rate with  $m_p$  being the proton mass and  $\eta$  being the accretion luminosity efficiency. Over an AGN disk lifetime of  $\tau_{\rm AGN} \sim 10\,{\rm Myr}$ , we can neglect gas accretion onto BHs on retrograde orbits.

In Table 2, we list parameter ranges for BH masses on the basis of the probabilistic toy model outlined above for three different assumptions: (1)  $N_{\rm BH} \propto M^{-2}$  (roughly the blue curve in Figure 1), corresponding to a short-lived disk with  $f_{\rm co} \gg f_{\rm g}$ . (2)  $N_{\rm BH} \propto M^{-1}$ , corresponding either to a long-lived disk  $(\tau_{\rm AGN} > 10~{\rm Myr})$  or efficient gas hardening with a low rate of orbit grind down  $(f_{\rm co} \gg f_{\rm g})$ . (3)  $N_{\rm BH} \propto M^{-2}(M^{-1.5})$  for  $M < 15~M_{\odot}(>15~M_{\odot})$ , corresponding either to efficient orbit grind down  $(f_{\rm g} \sim f_{\rm co})$ , or efficient stellar formation and evolution in the disk with a new top-heavy IMF. In Table 2, we list the binary mass ratio  $M_b$  range for each set of assumptions. The lower limit to  $M_b$  is trivially the lowest possible mass binary drawn from the initial mass distribution, with no growth from gas accretion and the upper limit to  $M_b$  is

Table 2
Parameter Ranges in BH Masses

Parameter	Lower	Upper
(1)	(2)	(3)
$M_b (M_{\odot})(\gamma = 2)$	10	100
$M_b (M_{\odot})(\gamma = 1)$	10	500
$M_b (M_{\odot})(\gamma = broken)$	10	500
$q(\gamma = 2)$	0.1	1
$q(\gamma = 1)$	0.01	1
$q(\gamma = broken)$	0.01	1

**Note.** Parameter ranges predicted for BH binaries in this channel, assuming initial BH mass range 5–15  $M_{\odot}$  and uniform distribution of BHs (see the text).

simply the highest mass binary in the distribution. Also listed in Table 2 are the range of mass ratios (q) of the binaries in the three different scenarios, with the lower limit given by the range of BH masses allowed in the three different distributions and q=1 is the trivial upper limit. Note that our assumption of  $5-15\,M_{\odot}$  initial mass BHs is conservative (Rodriguez et al. 2016a; Wang et al. 2016). In Secunda et al. (2018), we chose a wider range of initial BH masses  $5-30 M_{\odot}$  resulting in faster migration rates for the objects with  $M > 15 M_{\odot}$  in the same disk model and a more rapid binary formation (and merger) rate. However, our overall conclusions (e.g., on merger rate or spin distribution) are not affected much by this, since if mergers happen more quickly and masses end up in the migration trap faster, then the rate limiting factor is the lifetime of the AGN and the efficiency of the grind-down of the orbits by the disk. Essentially the rate is averaged over the lifetime of the AGN regardless of whether there's a runaway series of mergers in a short fraction of the AGN lifetime or it takes the entire lifetime to generate the same number of mergers.

If the fraction of BHs ground down into the disk  $f_{\rm g}(t) \geqslant f_{\rm co}(t)$ , the fraction of BHs coincident with the disk, which will be true for relatively long-lived, thin  $(h/R \ll 1)$  disks, the BH mass spectrum evolves from an initial power-law distribution to a broken power law as in Equation (5) with  $\gamma_1 \sim \gamma_0 > \gamma_2$ . The uncertainty in mass estimates for this channel is driven mainly by the initial mass distribution of BHs in the central region, as well as the ratio of  $f_{\rm g}(t)/f_{\rm co}(t)$ , which in turn depends on disk density and h/R.

## 5. Range of BH Spins

As BHs in the AGN disk accrete gas and merge with each other, their initial spin distribution will change with time. Assuming an initial even or flat distribution of spins (a) between a = [-1, +1] from which BH spin can be randomly drawn and angular momenta (L) for BHs in galactic nuclei, there will be four distinct populations of BHs in AGN disks as follows:

- 1. Prograde spin, on prograde orbits, denoted by  $(a^+, L^+)$ .
- 2. Prograde spin, on retrograde orbits  $(a^+, L^-)$ .
- 3. Retrograde spin, on prograde orbits  $(a^-, L^+)$ .
- 4. Retrograde spin, on retrograde orbits  $(a^-, L^-)$ .

We expect the fraction  $f_{co}$  of BHs co-orbital with the AGN disk should have an initial even (uniform) distribution across all four BH populations.

The four BH populations will evolve differently due to gas accretion. The  $(a^+, L^+)$  population rapidly accretes gas, spins

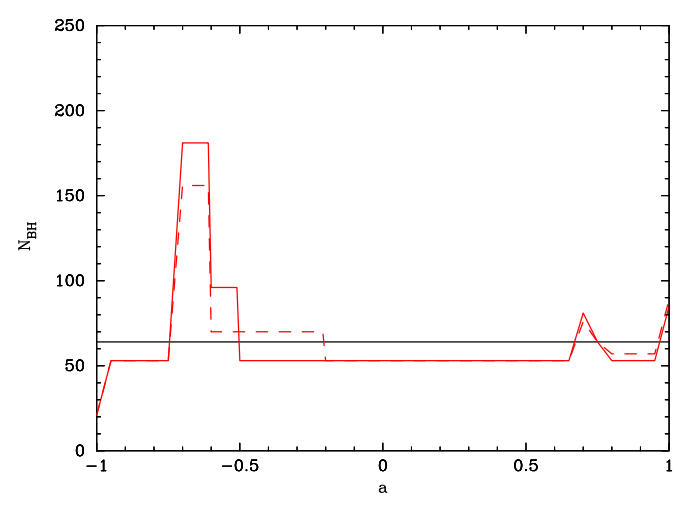


**Figure 2.** Evolution of an initial BH spin distribution (drawn randomly from a uniform spin distribution) in an AGN disk based on a toy merger model, including gas accretion (see the text). Spins are binned per 0.05 of spin parameter (a). Black line corresponds to a uniform BH spin distribution for the initial population. The corresponding initial mass distribution is given by the black curve in Figure 1. The red solid curve shows the spin distribution after the toy model has evolved for  $\Delta t \approx 0.1$ –0.3 Myr to include mergers and gas accretion at the Eddington rate. The corresponding mass distribution after this time is given by the red curve in Figure 1. The red dashed curve is the same as the solid curve, except we assume super-Eddington accretion at  $\times 5$  the Eddington rate.

up, and aligns spins with the disk gas once the BH has accreted a few percent of its own mass (Bogdanovic et al. 2007), i.e., in  $<\tau_{\rm AGN}$ . An initially uniform spin distribution  $a^+=[0,+0.98]$  evolves toward  $a^+\sim 0.98$  at an average rate  $\sim (\tau_{\rm AGN}/40~{\rm Myr})(\dot{m}/\dot{M}_{\rm Edd})$  where  $\dot{m}/\dot{M}_{\rm Edd}$  is the average gas accretion rate as a fraction of the Eddington rate (which takes  $\approx 40~{\rm Myr}$  to double mass). By contrast, the  $(a^+, L^-)$  population faces a strong headwind, so it accretes very weakly from the gas. An initially uniform distribution of spins in this population will remain uniform over  $\tau_{\rm AGN}$ . The  $(a^-, L^+)$  population spins down toward  $a\sim 0$  after an increase of mass by a factor  $\sqrt{3/2}$  (Bardeen 1970) and will then join the  $(a^+, L^+)$  population. The  $(a^-, L^-)$  population spins down more slowly due to the headwind and so an initial uniform distribution of spins remains uniform over  $\tau_{\rm AGN}$ .

BH mergers will further complicate the spin evolution of the four BH populations. The four populations interact due to migration and form binaries if captured within the binary Hill sphere. Binary orbital angular momentum  $(L_b)$  is the dominant contributor to the spin of the merged BH binary so equal mass BH mergers yield merger products with  $|a| \sim 0.7$  (Hofmann et al. 2016). Binaries can form with prograde or retrograde orbital angular momentum compared to the disk gas (denoted by  $L_b^{\pm}$ ). If a binary forms with retrograde orbital angular momentum  $(L_b^-)$ , the merger is faster than in the prograde case (Baruteau et al. 2011), and the merger product will have  $a^- = -0.7$  (i.e., retrograde spin compared to disk gas). Thus the fastest growing of the four populations of BHs in the disk due to mergers will actually be  $(a^-, L^{\pm})$ . This population evolves toward low spin  $(a \sim 0)$  due to gas accretion, at an average rate  $\sim (\tau_{\rm AGN}/40~{\rm Myr})(\dot{m}/\dot{M}_{\rm Edd})$ . Among the initial fraction  $f_{co}$  of co-orbital BHs, we expect equal numbers of prograde to retrograde orbits. However, since prograde orbits are ground down faster (smaller headwind, greater Bondi radius), we expect  $(a^{\pm}, L^{+})/(a^{\pm}, L^{-}) \approx 1 + (f_g/f_{co})$ .

Applying all of this to our toy model above allows us to construct the spin distribution in Figure 2. An initial spin distribution (black line), corresponding to a population randomly drawn from an underlying uniform distribution of spins evolves toward the solid red curve after  $\Delta t \approx$ 0.1-0.3 Myr. The corresponding mass distribution is the red curve in Figure 1. The red solid curve in Figure 2 shows a prominent peak at a = -0.7 due to a  $\times 5$  faster merger rate of retrograde binaries and a smaller peak at a = +0.7 due to mergers of prograde binaries. Both peaks are smeared out toward the right by gas accretion during  $\Delta t$  and will consist of BH masses  $\geq 10 \, M_{\odot}$  from the initial mass distribution. Some pile-up is happening at a > 0.95 due to gas accretion onto the already near maximal spinners of the  $(a^+, L^+)$  population. The red dashed curve shows what happens if we assume gas accretion can occur at super-Eddington rates onto BHs in the disk (×5 the Eddington rate). In particular, the more massive merged population at  $a \sim -0.7$  gets quickly smeared out and driven toward low spin. Thus, from Figure 2 if LIGO constrains the spins of most merger precursor BHs to be small, the AGN channel requires super-Eddington accretion onto initially retrograde spin BHs to grow this population. Note that we have ignored complications due to, e.g., likely binary mergers between BHs and stars in the disk, since the net effect of an interaction between the BH embedded in a stellar envelope could act to spin up or down the BH in an unpredictable way. Such interactions will tend to broaden the peak in our toy model distributions at  $a \sim \pm 0.7$  in Figure 2.

Only the  $(a^+, L^+)$  population will align or antialign relatively quickly with the AGN disk gas. Assuming the  $(a^+, L^+)$  populations are all aligned or antialigned with the disk gas, by drawing randomly from a uniform distribution across  $(a^\pm, L^\pm)$ , there is a  $\approx 1/16$  chance that both BHs have (anti)aligned spins and represent our lower limit for the fraction of BH (anti) aligned with disk gas. If  $f_g(t) \gg f_{co}(t)$ , then effectively the two populations  $(a^\pm, L^+)$  will dominate so  $f_{\pm align} \approx 1/4$ , which is our approximate upper limit for the fraction of BH (anti)aligned with disk gas. Our estimates of  $f_{\pm align}$  suggest that a larger population of mergers will be required to test this channel in population spin studies than estimated by Fishbach et al. (2017) and Gerosa & Berti (2017). Antialigned binaries in the AGN disk allow LIGO a unique chance to test the spin precession instability (Gerosa et al. 2015).

Once a BH binary merges, the resulting merger product can experience a gravitational radiation recoil kick of  $v_{
m kick} \sim$ 20–400 km s<sup>-1</sup>, depending on relative spins and mass ratios (e.g., Merritt et al. 2004; Campanelli et al. 2007). The result of kicks from mergers between aligned and antialigned objects is to incline the merger product's orbit relative to the AGN disk by  $\theta = \tan^{-1}(v_{\text{kick}}/v_{\text{orb}})$ , where  $v_{\text{orb}}$  is the orbital velocity of the binary center of mass. Since  $v_{\rm orb} \gg 400 \, {\rm km \, s^{-1}}$  in most of the disk, the orbital inclination perturbation is at most a few degrees and the merger product could be ground back down into the disk in time  $<\tau_{AGN}$ . Mergers of BHs with spins out of alignment with the plane of the disk and each other can produce the largest magnitude kicks (up to several thousand kilometers per second) (e.g., Schnittman & Buonanno 2007; Lousto et al. 2012). Such mergers will be rare, but will produce large kicks  $(\propto q^2/(1+q)^4$  in the mass ratio q, Campanelli et al. (2007), escape the disk at angle  $\theta$  and may not be ground back down within  $\tau_{AGN}$ .

Table 3
Parameter Ranges in BH Spins

Parameter (1)	Lower (2)	Upper (3)
$\frac{a^+(L^+)}{a^+(L^+)}$	0	0.98
$a^{-}(L^{+})$	-0.98	0
$a^{+}(L^{-})$	0.0	0.98
$a^{-}(L^{-})$	-0.98	0
$a_{\text{merge}}$	-0.7	+0.7
$f_{\pm  ext{align}}$	0.06	0.25

**Note.** Parameter ranges allowed for BH spins in this channel (see the text).

Table 3 summarizes the ranges allowed for spins in this LIGO channel. The typical spin distribution depends on the relative fractions of the four populations of BHs in the disk  $(a^{\pm}, L^{\pm})$  and their evolution as  $f_g/f_{co}$  changes, driven in turn by disk aspect ratio (h/R) and the disk gas density and  $\tau_{AGN}$ . We expect an initial population uniform across  $(a^{\pm}, L^{\pm})$ , but  $(a^{\pm}, L^{+})$  will grow with the fraction  $f_g(t)$  of BHs ground down into the disk. Peaks will arise in the spin distribution at  $a \sim -0.7$ , +0.7 due to mergers and gas accretion will drive  $a^{-} \rightarrow 0$  and  $a^{+} \rightarrow 0.98$  independent of mergers. Gas accretion at super-Eddington rates plus faster mergers by retrograde binaries may be required to generate a population of overweight, low spin BHs in the AGN disk.

#### 6. Observational Constraints: GW

Binary BH mergers in an AGN disk imply unique, testable predictions that would not be expected from other BH merger channels, including: (1) A spin distribution (see Section 5) that includes aligned/antialigned spin binaries and (2) a population of overweight BHs or IMBHs orbiting SMBHs, generating GWs detectable with the Laser Interferometer Space Antenna (LISA; McKernan et al. 2014). A circularized IMBH–SMBH binary at a migration trap  $(a_b \sim 10^2 r_g)$  around an SMBH with  $M_{\rm SMBH} < 10^7 M_{\odot}$  will be detectable with LISA at modest signal-to-noise ratio in a year's observation (McKernan et al. 2014). If AGN disks are efficient at gas-driven mergers of BHs, we expect that every AGN must contain one or more IMBH–SMBH binaries, implying an approximate rate comparable to that in Portegies Zwart et al. (2006).

### 7. Observational Constraints: EM

The brightest AGNs are too bright compared to any shortterm EM signal that might result from a BH merger in a gas disk. Low luminosity AGNs might permit short timescale EM events from BH mergers to be visible. As IMBHs grow in migration traps, gaps and cavities in the accretion flow can form and oscillations on the dynamical timescale of the accreting IMBH can be detected in optical, UV, and X-ray spectral signatures (e.g., McKernan et al. 2013, 2014; McKernan & Ford 2015). Temporal and energetic asymmetries in the X-ray signatures are best detected using microcalorimeters, such as the one that will fly on the X-ray Astronomy Recovery Mission succeeding Hitomi. Perturbations of the innermost disk will occur as migrators in the disk plunge into the SMBH and temporarily dominate the local corotating mass, detectable in large UV-optical quasar surveys (Drake et al. 2009) as well as the X-ray band. Large optical surveys of quasar disks can also limit total supernova rates due to migrating/accreting/colliding stars (Graham et al. 2017), in turn placing limits on the disk populations of stars and stellar remnants. Estimates of the rates of transits by bloated stars, best detected in the X-ray band (McKernan & Yaqoob 1998), can put limits on the population on spherical orbits around and passing through AGN disks.

As the AGN phase ends, the remaining BHs will interact dynamically, so the distribution of orbital parameters of the BHs and stars entrained in the disk will relax. Alexander et al. (2007) show that if very massive stars ( $>10^2\,M_\odot$ ) exist in our own Galactic nucleus, they can pump the eccentricity distribution of massive stars to even  $e \sim 0.4$  within 5 Myr. However, such stars are short lived and observed stellar eccentricities reach  $e \sim 0.7$  (Paumard et al. 2006). On the other hand, a population of overweight BHs caused by merger in an AGN disk can rapidly pump stellar orbital eccentricites post-AGN and inflate the thickness (h/R) of stellar disks in galactic nuclei. Thus, if this BH merger channel is efficient, thin disks of stars will not be observed in post-AGN galactic nuclei.

Neutron stars (NS) should also exist in AGN disks, and can migrate. So there should be a correlation between NS-NS and NS-BH mergers in AGN disks and the rate of BH-BH mergers expected from this channel. No correlation has been observed so far between short gamma-ray bursts in the local universe and AGNs (Berger 2014), but so far, only a handful of short gamma-ray bursts have sufficiently accurate positions in the sky to rule out an association with AGNs in these cases. The efficiency of this LIGO channel could be further constrained by ongoing studies of the correlation of short gamma-ray bursts with AGNs. Future simulations could usefully focus on the expected distribution of NSs in mass segregating clusters in galactic nuclei, and ultimately on determining the expected NS merger rate in AGN disks.

### 8. Conclusions

We parameterize the rate of BH mergers within AGN disks and the mass and spin distributions that result. The strongest observational constraints can be placed on this channel by: (1) ruling out a population of maximal spin BHs via LIGO, (2) ruling out a correlation between short gamma-ray bursts and AGNs, (3) constraining the rate of obscured supernovae in AGN disks via studies of large samples of AGNs, (4) ruling out a population of high accretion rate ADAFs in galactic nuclei, and (5) observing very thin disks of stars in nearby Galactic nuclei. Future simulations should focus on (1) the ratio of NS/BH in nuclear star clusters undergoing mass segregation, (2) encounters between prograde and retrograde orbiters in AGN disks, and (3) interactions and binary formation between BHs with pro- and retrograde spins and orbits at migration traps in a range of AGN disk models. If AGNs are efficient at merging BHs, LISA will detect a large population of IMBHs in disks around SMBHs in the nearby universe.

Thanks are due to Maya Fishbach, Davide Gerosa, Matthew Graham, Daniel Holz, Dan Stern, and Nick Stone for useful conversations. B.M. and K.E.S.F. are supported by NSF PAARE AST-1153335 and NSF PHY11-25915. B.M. and K.E.S.F. thank CalTech/JPL and NASA GSFC for support during sabbatical. M.-M.M.L. was partly supported by NSF AST11-09395.

#### ORCID iDs

Barry McKernan https://orcid.org/0000-0002-9726-0508

Z. Haiman https://orcid.org/0000-0003-3633-5403

B. Kocsis https://orcid.org/0000-0002-4865-7517

W. Lyra https://orcid.org/0000-0002-3768-7542

B. Metzger https://orcid.org/0000-0002-4670-7509

#### References

```
Abbott, B. P., Abbott, R., Abbott, T. D., et al. 2016a, PhRvL, 116, 241102
Abbott, B. P., Abbott, R., Abbott, T. D., et al. 2016b, ApJL, 833, L1
Alexander, R. D., Begelman, M. C., & Armitage, P. J. 2007, ApJ, 654, 907
Antonini, F. 2014, ApJ, 794, 106
Antonini, F., & Rasio, F. 2016, ApJ, 831, 187
Baldry, I. K., Driver, S. P., Loveday, J., et al. 2012, MNRAS, 421, 621
Bardeen, J. M. 1970, Natur, 226, 64
Bartos, I., Kocsis, B., Haiman, Z., & Márka, S. 2017, ApJ, 835, 165
Baruteau, C., Cuadra, J., & Lin, D. N. C. 2011, ApJ, 726, 28
Belczynski, K., Bulik, T., Fryer, C. L., et al. 2010, ApJ, 714, 1217
Bellovary, J., Mac Low, M.-M., McKernan, B., & Ford, K. E. S. 2016, ApJL,
  819, L17
Berger, E. 2014, ARA&A, 52, 43
Bogdanovic, T., Reynolds, C. S., & Miller, M. C. 2007, ApJL, 661, L147
Breen, P. G., & Heggie, D. C. 2013, MNRAS, 432, 2779
Campanelli, M., Lousto, C. O., Zlochower, Y., & Merritt, D. 2007, PhRvL, 98,
Cole, S., Norberg, P., Baugh, C. M., et al. 2001, MNRAS, 326, 255
deMink, S., & Mandel, I. 2016, MNRAS, 460, 3545
Drake, A. J., Djorgovski, S. G., Mahabal, A., et al. 2009, ApJ, 696, 870
Fishbach, M., Holz, D. E., & Farr, B. 2017, ApJL, 840, L24
Generozov, A., Stone, N. C., Metzger, B. D., & Ostriker, J. P. 2018, MNRAS,
   478, 4030
Georgakakis, A., Buchner, J., Salvato, M., et al. 2015, MNRAS, 453, 1946
Gerosa, D., & Berti, E. 2017, PhRvD, 95, 124046
Gerosa, D., Veronesi, B., Lodato, G., & Rosotti, G. 2015, PhRvL, 115, 141102
Graham, M., Djorgovski, S. G., Drake, A. J., et al. 2017, MNRAS, 470, 4112
Haehnelt, M. G., & Rees, M. 1993, MNRAS, 263, 168
Hailey, C. J., Mori, K., Bauer, F. E., et al. 2018, Natur, 556, 70
Haiman, Z., Kocsis, B., & Menou, K. 2009, ApJ, 700, 1952
Ho, L. C. 2008, ARA&A, 46, 475
Hofmann, F., Barausse, E., & Rezzolla, L. 2016, ApJL, 825, L19
Hopman, C., & Alexander, T. 2006, ApJL, 645, L133
Horn, B., Lyra, W., Mac Low, M.-M., & Sándor, Z. 2012, ApJ, 750, 34
Kennedy, G., Meiron, Y., Shukirgaliyev, B., et al. 2016, MNRAS, 460,
King, A., & Nixon, C. J. 2015, MNRAS, 453, L46
```

Kocsis, B., Yunes, N., & Loeb, A. 2011, PRD, 84, 024032

```
Lasota, J.-P., Vieira, R. S. S., Sadowski, A., Narayan, R., & Abramowicz, M. A.
  2016, A&A, 587, 13
Leigh, N. W. C., Antonini, F., Stone, N. C., Shara, M. M., & Merritt, D. 2016,
      VRAS, 463, 1605
Leigh, N. W. C., Geller, A. M., McKernan, B., et al. 2017, MNRAS, 474, 5672
Lousto, C. O., Zlochower, Y., Dotti, M., & Volonteri, M. 2012, PRD, 85,
McKernan, B., & Ford, K. E. S. 2015, MNRAS, 452, L1
McKernan, B., Ford, K. E. S., Kocsis, B., & Haiman, Z. 2013, MNRAS,
  432, 1468
McKernan, B., Ford, K. E. S., Kocsis, B., Lyra, W., & Winter, L. M. 2014,
    INRAS, 441, 900
McKernan, B., Ford, K. E. S., Lyra, W., et al. 2011, MNRAS, 417, L103
McKernan, B., Ford, K. E. S., Lyra, W., & Perets, H. B. 2012, MNRAS,
  425, 460
McKernan, B., & Yagoob, T. 1998, ApJL, 501, L29
Merritt, D., Milosavljević, M., Favata, M., Hughes, S. A., & Holz, D. E. 2004,
    ApJL, 607, L9
Miller, M. C., & Davies, M. B. 2012, ApJ, 755, 81
Miralda-Escudé, J., & Gould, A. 2000, ApJ, 545, 847
Morris, M. 1993, ApJ, 408, 496
Narayan, R., & Yi, I. 1995, ApJ, 444, 231
O'Leary, R. M., Kocsis, B., & Loeb, A. 2009, MNRAS, 395, 2127
O'Shaughnessey, R., Gerosa, D., & Wysocki, D. 2017, PhRvL, 119, 1101
Paardekooper, S.-J., Baruteau, C., Crida, A., & Kley, W. 2010, MNRAS,
  401, 1950
Paczynski, B., & Witta, P. J. 1980, A&A, 88, 23
Paumard, T., Genzel, R., Martins, F., et al. 2006, ApJ, 643, 1011
Portegies Zwart, S. F., Baumgardt, H., McMillan, S. L. W., et al. 2006, ApJ,
  641, 319
Reines, A. E., & Volonteri, M. 2015, ApJ, 813, 82
Rodriguez, C. L., Amaro-Seoane, P., Chatterjee, S., & Rasio, F. A. 2018,
   PhRvL, 120, 151101
Rodriguez, C. L., Chatterjee, S., & Rasio, F. A. 2016a, PhRvD, 93, 084029
Rodriguez, C. L., Haster, C.-J., Chatterjee, S., Kalogera, V., & Rasio, F. A.
  2016b, ApJL, 824, L8
Samsing, J., MacLeod, M., & Ramirez-Ruiz, E. 2014, ApJ, 784, 71
Sánchez-Salcedo, F. J., & Chametla, R. O. 2014, ApJ, 794, 167
Schawinski, K., Koss, M., Berney, S., & Sartori, L. F. 2015, ApJ, 451, 2517
Schnittman, J. D., & Buonanno, A. 2007, ApJL, 662, L63
Secunda, A., Adorno, J., Bellovary, J., et al. 2018, ApJ, submitted (arXiv:1807.
  02859)
Sirko, E., & Goodman, J. 2003, MNRAS, 341, 501
Stahler, S. W. 2010, MNRAS, 402, 1758
Stone, N. C., Metzger, B. D., & Haiman, Z. 2017, MNRAS, 464, 946
Thompson, T. A., Quataert, E., & Murray, N. 2005, ApJ, 630, 167
Volonteri, M., Dubois, Y., Pichon, C., & Devriendt, J. 2016, MNRAS,
  460, 2979
Wang, L., et al. 2016, MNRAS, 458, 1450
```

Kroupa, P. 2002, Sci, 295, 82